

# Elaboration and optimization of (Y,Er)Al<sub>3</sub>(BO<sub>3</sub>)<sub>4</sub> glassy planar waveguides through the sol–gel process

L.J.Q. Maia<sup>a,\*</sup>, J. Fick<sup>b</sup>, C. Bouchard<sup>b</sup>, V.R. Mastelaro<sup>c</sup>, A.C. Hernandez<sup>c</sup>, A. Ibanez<sup>b</sup>

<sup>a</sup> Grupo Física de Materiais, IF – Universidade Federal de Goiás, Caixa Postal 131, 74001-970 Goiânia/GO, Brazil

<sup>b</sup> Institut Néel, CNRS and Université Joseph Fourier, 25 Avenue des Martyrs, BP 166, 38042 Grenoble, France

<sup>c</sup> Grupo Crescimento de Cristais e Materiais Cerâmicos, IFSC – Universidade de São Paulo, Caixa Postal 369, 13560-970 São Carlos/SP, Brazil

## ARTICLE INFO

### Article history:

Received 22 June 2009

Received in revised form 27 September 2009

Accepted 23 October 2009

Available online 1 December 2009

### PACS:

77.55.+f

78.20.–e

78.20.Ci

78.66.–w

### Keywords:

Thin films

Y<sub>0.9</sub>Er<sub>0.1</sub>Al<sub>3</sub>(BO<sub>3</sub>)<sub>4</sub>

Sol–gel process

Structural and optical properties

Waveguiding properties

## ABSTRACT

In this work, a sol–gel route was used to prepare Y<sub>0.9</sub>Er<sub>0.1</sub>Al<sub>3</sub>(BO<sub>3</sub>)<sub>4</sub> glassy thin films by spin-coating technique looking for the preparation and optimization of planar waveguides for integrated optics. The films were deposited on silica and silicon substrates using stable sols synthesized by the sol–gel process. Deposits with thicknesses ranging between 520 and 720 nm were prepared by a multi-layer process involving heat treatments at different temperatures from glass transition to the film crystallization and using heating rates of 2 °C/min. The structural characterization of the layers was performed by using grazing incidence X-ray diffraction and Raman spectroscopy as a function of the heat treatment. Microstructural evolution in terms of annealing temperatures was followed by high resolution scanning electron microscopy and atomic force microscopy. Optical transmission spectra were used to determine the refractive index and the film thicknesses through the envelope method. The optical and guiding properties of the films were studied by *m*-line spectroscopy. The best films were monomode with 620 nm thickness and a refractive index around 1.664 at 980 nm wavelength. They showed good waveguiding properties with high light-coupling efficiency and low propagation loss at 632.8 and 1550 nm of about 0.88 dB/cm.

© 2009 Elsevier B.V. All rights reserved.

## 1. Introduction

In the last 10 years, a great attention has been done to the development of efficient and compact optical waveguide amplifiers and lasers in rare earth doped-glasses for integrated optical devices [1–3]. Among the rare-earth elements, Er<sup>3+</sup> ion with 1540 nm photoluminescence emission is of particular interest for optical amplification in telecommunications. In order to make a compact amplifier, a few centimeters long, a high erbium concentration is required when compared with erbium doped fiber amplifiers involving typically several meters in length. However, due to the onset of concentration quenching at low doping levels in silica, the relatively low gain unit length which can be achieved has made such development difficult. Thus, there is a great interest to develop other amorphous host matrices with high solubility of rare-earth elements, especially erbium, for integrated systems [4].

On the other hand, borate materials are of interest due to their wide UV transparency and their non-linear properties associated to

high optical damage thresholds [5,6]. Many of them, such as YBO<sub>3</sub>, LaBO<sub>3</sub>, GdBO<sub>3</sub>, and Y<sub>3</sub>BO<sub>6</sub> are also good host matrices for active luminescent rare earth ions [5,7,8].

The Yttrium aluminum borate matrix (YAl<sub>3</sub>(BO<sub>3</sub>)<sub>4</sub>, YAB) is one of the potential host candidates. In the crystal form, it exhibits good properties for solid-state lasers: high physical and chemical stability, high thermal conductivity and good mechanical strength [9]. YAB can be also used for waveguiding. Indeed, its high refractive index ( $n = 1.6–1.7$ ) compared to silica substrate ( $n = 1.45$ ) allows to realize a large angle of light admittance and a high light confinement, thus increasing the pump absorption and amplification efficiencies [10].

Our purpose was to obtain homogeneous glassy thin films to develop waveguides without grain boundaries which lead to high optical losses in polycrystalline films. Erbium-doped YAB composition appears as a suitable host matrix for efficient integrated optical amplifiers due to its high rare-earth solubility, high glass transition temperature  $T_g$ , around 746 °C, and good thermal stability versus crystallization [11].

In a previous work, stable sols were successfully prepared by the sol–gel process [11]. The sol–gel technique is considered as a

\* Corresponding author. Tel.: +55 62 35211122x206; fax: +55 62 35211014.  
E-mail address: [lauro@if.ufg.br](mailto:lauro@if.ufg.br) (L.J.Q. Maia).

low cost deposition method which allows obtaining planar waveguides of high optical quality. Advantages of this method are the high control of chemical purity, low temperature of synthesis, easy incorporation of rare earth ions and the possibility to cover large substrates area by the spin-coating technique [12]. Likewise, the sol–gel process appears to be quite attractive for the preparation of multi-component systems as it's allows homogeneous reactions in solution of all the precursors at the molecular level. A new sol-gel route was developed by our group, in which  $Y_{0.9}Er_{0.1}Al_3(BO_3)_4$  crystalline and amorphous powders and films were demonstrated to be synthesized with good optical quality [11,13]. The glass transition and crystallization temperatures of this matrix were found around 746 °C and 830 °C, respectively. In this previous work, only single-layer films were elaborated and the deposition conditions were optimized with regard to the sol chemistry. In the present work the elaboration and optimization of multi-layers thin films is presented. The waveguiding properties of these films were investigated, as well as the heat-treatment suitable to obtain amorphous and dense films without cracks and pores. This work was also devoted to optimize the structural, microstructural and optical properties of the thin films by using X-ray diffraction, scanning electron and atomic force microscopies and optical transmission characterizations. Moreover, the refractive index dispersion in the visible and near infrared regions was determined by the envelope method applied on the transmission spectra. Finally, *m*-line spectroscopy was used for determining the waveguiding properties such as refractive index, propagation modes and losses.

## 2. Experimental procedure

### 2.1. Sol synthesis and multi-layer depositions

Aluminum acetylacetonate ( $Al(acac)_3$ , Aldrich 99%), tri-*i*-propylborate ( $B(OPr^i)_3$ , Strem 98%), yttrium nitrate hexahydrate ( $Y(NO_3)_3 \cdot 6H_2O$ , Aldrich 99.9%), and erbium nitrate pentahydrate ( $Er(NO_3)_3 \cdot 5H_2O$ , Aldrich 99.9%), were used as precursors to obtain the  $Y_{0.9}Er_{0.1}Al_3(BO_3)_4$  solid solution phase by the sol–gel method. Ethyl alcohol ( $C_2H_5OH$ , Riedel-de Haen 99.8%), and propionic acid ( $C_2H_5CO_2H$ , PropAc, Merck 99%) were used as solvents. The preparation of the sols was performed in a dry glove box ( $N_2$  atmosphere). The precursor dissolution was first carried out in ethyl alcohol (EtOH) and propionic acid (PropAc) at 80 °C during 2 h in airtight silica cells to avoid any evaporation. Pure water was added for the hydrolysis at 80 °C during 1 h. In all our experiments, the relative molar amounts of cation precursors, corresponding to the YAB composition, and of water were fixed at 0.9 Y:0.1 Er:3 Al:4 B:55 PropAc:95 EtOH:5  $H_2O$ . For more details see Ref. [11]. The resulting sols were filtered at room temperature (26 °C) by using filters of 0.2  $\mu m$  porosity. During these heat treatments, the solution was placed into a closed silica glass flask with polypropylene cover. Finally, by removing the cover, the solvent were partially evaporated, around 65 vol.%, at 80 °C during 70 min. These concentrated solutions were used to prepare thin films by spin-coating deposited on silica glass and (1 0 0) silicon substrates. Before coating deposition, these substrates were cleaned by detergent (Argos, biodegradable anionic surfactant), rinsed with deionized water and then immersed in a  $HNO_3 + HCl$  (16  $HNO_3 + 28 HCl + 56 H_2O$  molar proportions) solution during 5 min. The substrates were rinsed again with deionized water and ethyl alcohol and finally dried through air flow. A spin-coater (RC8 SussMicrotech™) equipment involving the gyrset technology allowed to improve the film uniformity. Rotation acceleration, rotation speed and spinning time were fixed at 500 rpm/s, 2250 rpm, and 5 s, respectively. After the deposition of each layer, the films were dried at 80 °C for 30 min. Then, a first annealing at

400 °C during 2 h was applied with a heating rate of 1 °C/min while a second one (2 h at 700 °C) was achieved at 2 °C/min. This procedure was repeated for each layer (7-layers), and the resulting films were finally annealed under oxygen between 740 and 850 °C during 2 h with a heating rate of 1 °C/min.

### 2.2. Microstructural and structural characterizations

Grazing incidence X-ray diffraction (GIXRD) measurements were performed with a home made diffractometer using a PSD (position-sensitive detector) from Inel. The  $Fe K\alpha$  ( $\lambda = 1.936 \text{ \AA}$ ) radiation (34 kV/25 mA) with 2 mm divergence and 0.6 mm reception slits and a graphite monochromator were the main set of experimental parameters. The incident angle of X-ray beam was fixed at  $\theta_i = 0.5^\circ$ , the scan range ( $2\theta$ ) was fixed between 12 and 90° while the total collecting time of each GIXRD pattern was 7200 s.

Raman spectra were registered at room temperature using a micro-Raman Renishaw R2000 system. The samples were excited with a 632.8 nm He–Ne line and the Raman spectra collected between 1050 and 1800  $cm^{-1}$  with a spectral resolution of approximately 1  $cm^{-1}$ .

Surface quality and microstructure of the films were analyzed using a high resolution scanning electron microscope (HR-SEM) (FEG-VP Supra 35, Zeiss), while the surface morphology of the films was observed by an atomic force microscope (AFM – Digital instrument Nanoscope III) using the tapping mode to measure the surface root-mean-square (RMS) roughness and grain sizes.

### 2.3. Optical characterizations

Optical transmission spectra in the UV–Visible–NIR near regions (200–2000 nm) were recorded at room temperature using a Perkin–Elmer spectrophotometer (Lambda 9, 240 nm  $min^{-1}$ , resolution of 0.2 nm). Waveguiding properties were investigated by *m*-line spectroscopy [14] involving a symmetrical 60° prism (Schott SF 58 glass) with a refractive index  $n_p = 1.8736$  at the 980 nm wavelength. Loss measurements were recorded on 15 mm long samples by a scanning optical fiber probe moving along the length of the propagating light streak in a Metricon® equipment (model 2010). The attenuation coefficient was obtained by fitting the data with an exponential decay function, assuming a homogeneous longitudinal distribution of the scattering centers and a constant loss parameter for these planar waveguides. The measurements were performed by excitation of the fundamental transverse electric mode of the planar waveguide at 632.8 nm and 1550 nm.

## 3. Results and discussion

### 3.1. Structural characterizations

The GIXRD patterns of  $Y_{0.9}Er_{0.1}Al_3(BO_3)_4$  thin films deposited on silica substrates and annealed during 2 h at the final 780, 820, and 850 °C temperatures are presented in Fig. 1. One can observe that the films are amorphous below 820 °C while after an annealing at 820 °C, the resulting film is partially crystallized in the  $Al_4B_2O_9$  compound (JCPDS No. 09-0158). At 850 °C, two crystalline phases,  $Al_4B_2O_9$  (JCPDS Card No. 09-0158) and  $YBO_3$  (JCPDS Card No. 88-0356) coexist with a remaining amorphous phase. These results are in agreement with our previous results for the crystallization of fine amorphous  $Y_{0.9}Er_{0.1}Al_3(BO_3)_4$  powders prepared by the sol–gel process [11,13], and also, with those reported by Madarasz et al. [15]. They observed, for the YAB composition, the formation of  $Al_4B_2O_9$  by solid state reaction at 800 °C. On the other hand,

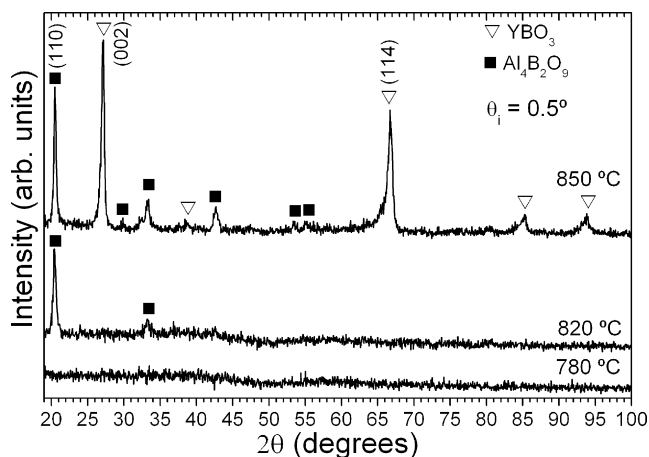


**Fig. 1.** GIXRD patterns of  $Y_{0.9}Er_{0.1}Al_3(BO_3)_4$  thin films (7-layers) coated on silica substrates and annealed at 780, 820, and 850 °C during 2 h with a heating rate of 2 °C/min.

the YAB or  $Y_{0.9}Er_{0.1}Al_3(BO_3)_4$  crystalline phases can be obtained only at high temperatures, around 1150 °C as previously reported by several works [11,13,15,16].

In order to better understand the structural changes occurring from amorphous (740 °C) to partially crystallized (850 °C)  $Y_{0.9}Er_{0.1}Al_3(BO_3)_4$  films deposited on silicon substrates, Raman spectroscopy was used. Raman spectra are illustrated in Fig. 2 between 1050 and 2250  $cm^{-1}$ . Spectra were not analyzed below 1050  $cm^{-1}$ , due to the presence of many silicon substrate bands overlapping with those of the films. Similar spectra were registered for films heat-treated at 740 and 780 °C during 2 h while a significant evolution is observed for films annealed at 820 and 850 °C. The 740 and 780 °C spectra were well deconvoluted by two Gaussians curves while four Gaussian curves were necessary for the 820 and 850 °C ones. Vibrational frequencies, area under each Gaussian peak and corresponding FWHM (Full width half maximum) are listed in Table 1.

Several crystalline and amorphous borates studies of known structures have shown that trigonal  $BO_3$  units have strong bands in the spectral range 1100–1600  $cm^{-1}$ , whose shape depends on the numbers of bridging and non-bridging oxygen and consequently differs for orthoborates, pyroborates, and metaborates linkages [17,18]. Tetrahedral  $BO_4$  units exhibit characteristic vibra-

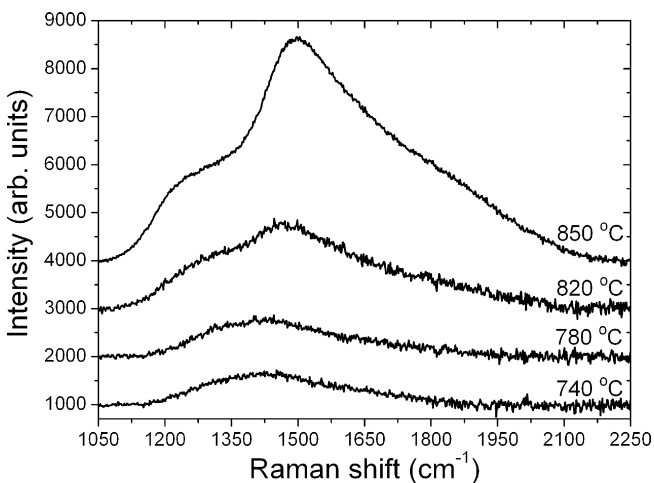


**Fig. 2.** Raman spectra of  $Y_{0.9}Er_{0.1}Al_3(BO_3)_4$  thin films (7-layers) deposited on silicon substrate and annealed 2 h at 740, 780, 820, and 850 °C.

**Table 1**

Vibrational band frequencies, normalized area and full-width at half medium (FWHM) of Raman spectra for the Er:YAB glassy thin films heat treated at different temperatures.

Heat treatment (°C)	Frequency ( $cm^{-1}$ )	Normalized area (%)	FWHM ( $cm^{-1}$ )
740	1385	59	107
	1594	41	134
780	1388	53	108
	1596	47	170
820	1292	24	80
	1450	24	68
	1566	16	83
	1721	36	173
850	1271	16	80
	1486	38	82
	1640	9	72
	1767	37	163

tions between 800 and 1200  $cm^{-1}$ . In this work the  $BO_3$  and  $BO_4$  groups could be analyzed through four band splitting due to different surroundings.

The main features in the Raman spectra of glassy  $Y_{0.9}Er_{0.1}Al_3(BO_3)_4$  thin films annealed at 740 and 780 °C (Fig. 2 and Table 1) are the bands centered around 1388 and 1596  $cm^{-1}$ , respectively. Slight differences in the spectra are observed from 740 to 780 °C that can be related to the structural relaxations associated to the glassy transition  $T_g \sim 746$  °C, while at higher temperatures, 820–850 °C, significant changes in band intensities and peak positions are due to the film crystallizations. Indeed, two new bands centered at 1292  $cm^{-1}$  and 1721  $cm^{-1}$  emerge due to the  $Al_4B_2O_9$  crystallization and a breakdown of  $BO_4$  units to form  $BO_3$  with bridging or non-bridging oxygens, respectively, in agreement with the previous results of Mazza et al. in the  $Al_2O_3$ – $B_2O_3$  system [19]. On the other hand, the bands centered at 1450 and 1566  $cm^{-1}$  can be assigned to the  $BO_4$  and  $BO_3$  units with non-bridging oxygens, respectively, of the amorphous remaining phase [13]. Also, these bands are related to the formation of  $YBO_3$  phase.

Finally, the band at 1721  $cm^{-1}$  is due to the stretching between boron and hydroxyl groups. Indeed, the crystallization induces a chemical instability, the rough surface of the film becoming slightly hygroscopic.

These results confirm the GIXRD results discussed above illustrating the glass network breakdown when the  $Al_4B_2O_9$  and  $YBO_3$  crystallization occurs.

### 3.2. Microstructural properties

The surface morphology of films on silicon substrates annealed 2 h between 740 and 850 °C was characterized by HRSEM (Fig. 3). From the micrograph (a), corresponding to an annealing at 780 °C, one can see that this glassy thin film is very homogeneous and does not exhibit any grains. Similar micrographs were recorded for annealing at 700 and at 740 °C. When the annealing temperature increases (Fig. 3b and c), we observe a non uniform surface with nanometer-sized grains according to the  $Al_4B_2O_9$  and  $YBO_3$  crystallizations (Fig. 1). Fig. 3d and e are the corresponding cross-sections of films which exhibit very good chemical homogeneity in thickness. The film annealed at 740 °C exhibits a good densification and do not present crystal grains or pores, but the cleavage process was not perfect due to the glassy state of the films 720 nm-thick. The film annealed at 780 °C, just above  $T_g$ , exhibits a higher densification with a perfect cleavage showing well uniform layer with a reduced thickness of 520 nm. At 820 °C (Fig. 3f), the film surface become very irregular due to the crystallization process inducing an irregular increase of the thickness, around 620 nm.

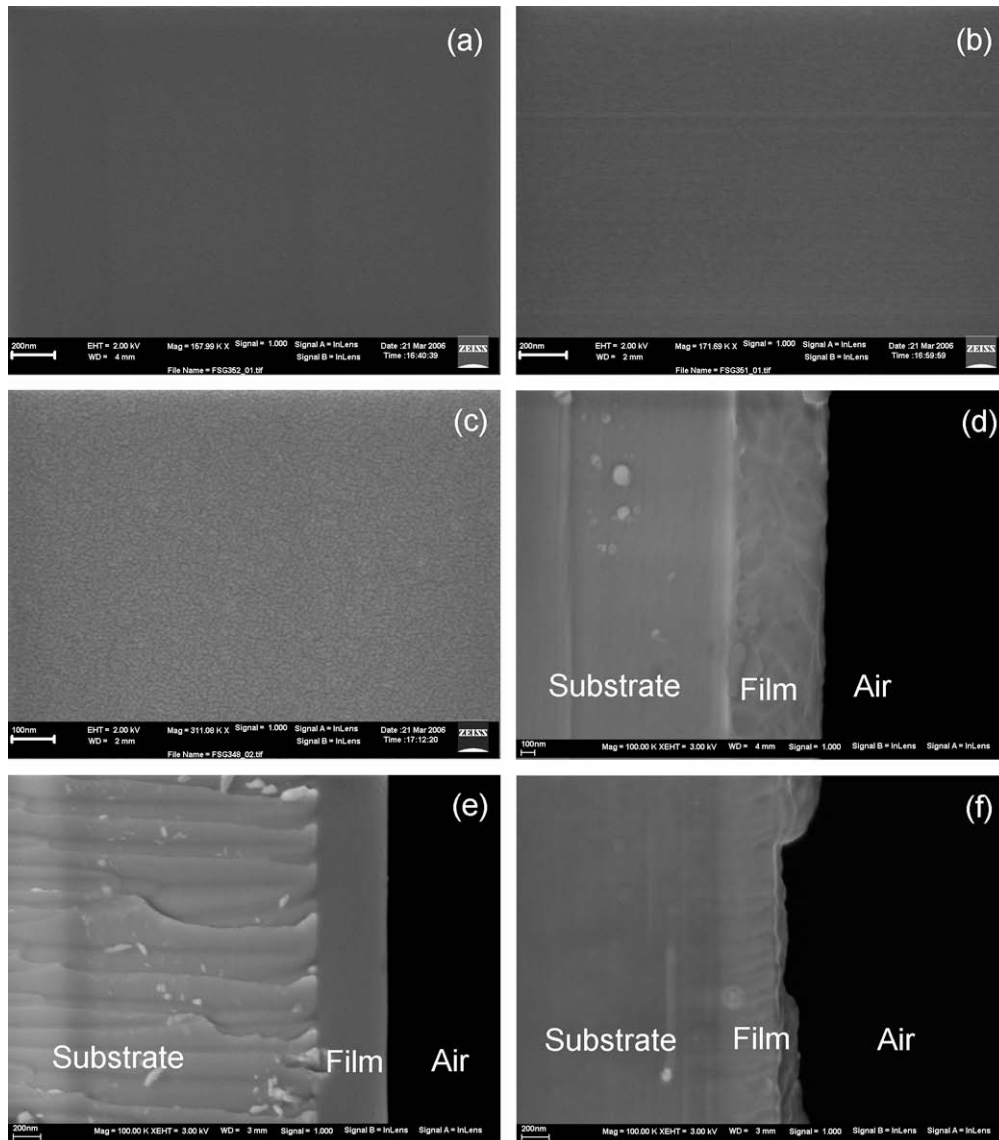


**Fig. 3.** HR-SEM surface micrographs of  $Y_{0.9}Er_{0.1}Al_3(BO_3)_4$  thin films (7-layers) on silicon substrate, annealed at 780 °C (a), 820 °C (b), and 850 °C (c) during 2 h using a heating rate of 2 °C/min. (d), (e) and (f) are HR-SEM cross-section micrographs of  $Y_{0.9}Er_{0.1}Al_3(BO_3)_4$  thin films annealed 2 h at 740 °C, 780 °C and 820 °C, respectively.

The films are amorphous  $Y_{0.9}Er_{0.1}Al_3(BO_3)_4$  composition at 700 °C, but the crystallization occurs first by the formation of  $Al_4B_2O_9$  (820 °C) phase followed by the crystallization of  $YBO_3$  phase (850 °C) while the coatings remain partly in the amorphous state. On the other hand, we have previously shown by thermogravimetry on the corresponding sol-gel powders [13] that a small boron oxide loss occurs during the crystallization at about 820–850 °C. We believe that two different effects occur simultaneously for the samples annealed at 820 and 850 °C: contraction of the crystallized areas and coating expansion or cracks due to the boron oxide losses at 820–850 °C leading thus to non-homogeneous film surfaces.

The film surface microstructure was also analyzed as a function of annealing temperatures by AFM (Fig. 4): at 740 °C the films exhibit non-homogeneous surfaces with roughnesses of about 0.6 nm RMS; at 780 °C film surfaces become very smooth (0.1 nm RMS); at 820 °C some crystal grains of  $75 \pm 3$  nm in diameter are formed thus rising the roughness to 0.6 nm RMS and finally at 850 °C, the grains grow, around  $82 \pm 4$  nm in diameter, leading to a higher roughness of 1.1 nm RMS due to the crystallization of  $Al_4B_2O_9$  and  $YBO_3$ . Thus, this microstructural study allowed to specify the

annealing temperature around 780 °C for the preparation of high quality thin films exhibiting high density and chemical homogeneity coupled to a very smooth surface that is required for the development of waveguide devices of low optical loss.

### 3.3. Optical transmission properties

Optical transmissions of glassy and partially crystallized thin films were measured continuously from 200 nm to 2000 nm. Fig. 5 displays the transmission spectra of films composed by seven multi-layers on silica substrate and heat-treated at different temperatures with a heating rate of 2 °C/min. First, a good transparency in the visible and near infrared regions (higher than 85%) is observed for all films. The films heat-treated at 740 °C do not present suitable interference fringes due certainly to some lack of homogeneity (Fig. 5a) while those sintered at 780 and 820 °C exhibit good interference spectra in agreement with the microstructural study. For films annealed at 850 °C, the UV transmission and interference amplitude in the visible are reduced. This feature is due to the Rayleigh scattering of  $Al_4B_2O_9$  and  $YBO_3$  crystal grains as previously observed by AFM (Fig. 4d). Consequently, the best transmission

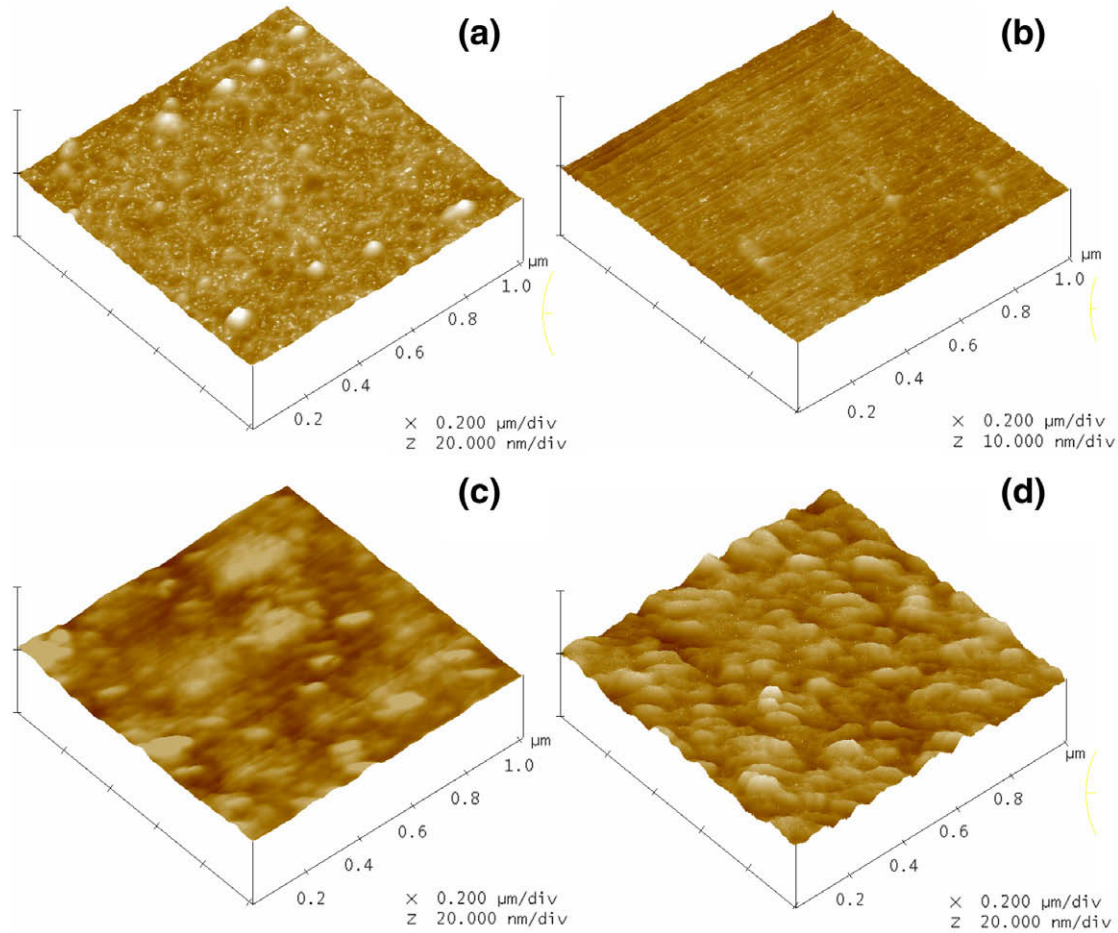


**Fig. 4.** 3D  $1 \times 1 \mu\text{m}^2$  AFM images of  $\text{Y}_{0.9}\text{Er}_{0.1}\text{Al}_3(\text{BO}_3)_4$  thin films (7-layers) on silicon substrate, annealed at 740 °C (a), 780 °C (b), 820 °C (c), and 850 °C (d) during 2 h using a heating rate of 2 °C/min.

spectra are obtained for films annealed between 780 and 820 °C confirming that the grain size and densification are crucial factors to prepare  $\text{Y}_{0.9}\text{Er}_{0.1}\text{Al}_3(\text{BO}_3)_4$  high quality thin films. The refractive index ( $n$ ) and film thickness were determined from the interference fringes by the envelope method, using the expression reported by Manificier et al. [20] and modified by Peng and Desu [21]:

$$n = \left[ N + (N^2 - n_s^2)^{1/2} \right]^{1/2} \quad (1)$$

where

$$N = \frac{1}{2} (1 + n_s^2) + 2n_s \left( \frac{T_{\max} - T_{\min}}{T_{\max} \cdot T_{\min}} \right) \quad (2)$$

where  $T_{\max}$  and  $T_{\min}$  are the transmission maximum and the corresponding minimum at the wavelength  $\lambda$  of the interference fringes (Fig. 5), while  $n_s$  is the substrate refractive index (silica [22]) at the same wavelength. The refractive index values, calculated from Eq. (1), are shown in Fig. 6a for  $\text{Y}_{0.9}\text{Er}_{0.1}\text{Al}_3(\text{BO}_3)_4$  films annealed at 780 °C. The refractive index results were fitted with the following Sellmeier curve [23,24]:

$$n^2 = A + \frac{B}{\lambda^2 - C} - D\lambda^2. \quad (3)$$

The fit of the experimental data provides the following set of parameters:  $A = 2.7711$ ,  $B = 0.0173$ ,  $C = 0.0073$  and  $D = 0.0275$  ( $\lambda$  in  $\mu\text{m}$ ). This Sellmeier fits very well the measured points, as can be seen in Fig. 6a. The refractive index dispersion of glassy films is slightly smaller than those reported for Er-doped YAB crystal [23].

Fig. 6b illustrates the thin film refractive index at  $\lambda = 980 \text{ nm}$  as a function of the annealing temperature. Clearly, the values exhibit a maximum at 780 °C corresponding to the highest densification and best homogenization of the film at an annealing temperature just above  $T_g$ . At higher temperatures, the crystallization onset in-

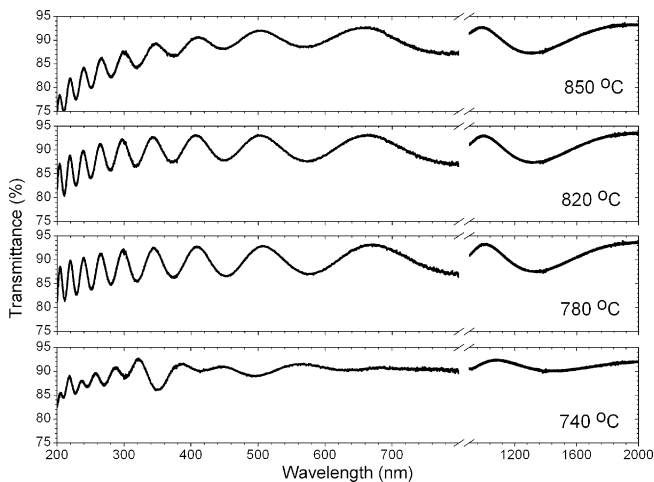


**Fig. 5.** UV-Visible-near IR optical transmission spectra of  $\text{Y}_{0.9}\text{Er}_{0.1}\text{Al}_3(\text{BO}_3)_4$  7-layers coated on silica substrate and annealed at different temperatures with a heating rate of 2 °C/min.

duces a decrease of the refractive index due to the formation of voids.

It is also possible to estimate the film thickness from the transmission spectra. The thickness  $d$  can be calculated from two adjacent maxima or minima of interference fringes at  $\lambda_1$  and  $\lambda_2$  by the equation [21,24]:

$$d = \frac{\lambda_1 \cdot \lambda_2}{[2(n(\lambda_1) \cdot \lambda_2 - n(\lambda_2) \cdot (\lambda_1))]} \quad (4)$$

where  $\lambda_1$ ,  $n(\lambda_1)$  and  $\lambda_2$ ,  $n(\lambda_2)$  are the corresponding wavelengths and refractive indexes calculated by the envelope method. The average  $d$  values are plotted in Fig. 6b as a function of the annealing temperature. In good agreement with the best film densification obtained at 780 °C, one can observe a thickness minimum between 780 and 820 °C. The  $\text{Al}_4\text{B}_2\text{O}_9$  crystallization, above 820 °C, induces an expansion of the layer due to the formation of crystal grains and voids.

According to Peng and Desu [21], the packing densities of films can be estimated from the Bruggeman [25] effective medium approximation. The packing densities of single phase porous films can be determined by the equation [21,24]:

$$f \frac{n_b^2 - n^2}{n_b^2 + 2n^2} + (1 - f) \frac{1 - n^2}{1 + 2n^2} = 0 \quad (5)$$

where  $f$  is the volume fraction or the packing density of the film,  $n_b$  is the refractive index of the bulk material (Er-doped YAB crystals

[23]), and  $n$  is the above determined refractive index. In this work, the refractive index of the films is smaller than that of Er-doped crystal due to the glassy network and the porosity of the films annealed above 780 °C. Table 2 summarizes the packing densities of  $\text{Y}_{0.9}\text{Er}_{0.1}\text{Al}_3(\text{BO}_3)_4$  films, calculated using the value of the extraordinary index of Er:YAB crystals. The packing densities indicate a maximum of densification at 780 °C, with a good packing of glassy films higher than 96%. This difference of 4% with the Er-doped YAB crystal can be related to structure distortions of aluminoborate glassy network, as well as to nanometer-sized porosity of the films. Thus, these results are in perfect agreement with all the previous ones presented above.

The film heat-treated at 780 °C is very promising for the design of waveguides with a high  $\Delta n = 0.21$  between the film and the  $\text{SiO}_2$  buffer layer (or cladding), such that a guiding layer thickness of  $620 \pm 10$  nm would already be sufficient for single mode propagation at 980 and 1540 nm wavelengths.

### 3.4. Waveguiding properties

The  $m$ -line spectra of  $\text{Y}_{0.9}\text{Er}_{0.1}\text{Al}_3(\text{BO}_3)_4$  thin films annealed at 740, 780 or 820 °C, are shown in Fig. 7. Only the fundamental  $\text{TE}_0$  and  $\text{TM}_0$  waveguide modes could be excited, suggesting that all waveguides are monomode. The measured effective index  $n_{\text{eff}}$  of the observed modes are reported in Table 3 as well as the linewidths (FWHM), and the coupling efficiency. The film refractive index was calculated using the standard guided mode dispersion equation [26] using a film thickness of 620 nm. One notes that the  $n_{\text{eff}}$  of the  $\text{TE}_0$  and  $\text{TM}_0$  modes have a maximum at 780 °C. At the same time, the coupling efficiency remains almost constant for 740 and 780 °C, but it decreases at 820 °C, specially for the  $\text{TM}_0$  mode due the partial coating crystallization. The best results are obtained for the film annealed at 780 °C with coupling efficiencies of 48% and linewidths of around 0.0013. The coupling efficiency is directly related to the waveguide losses and thus to the

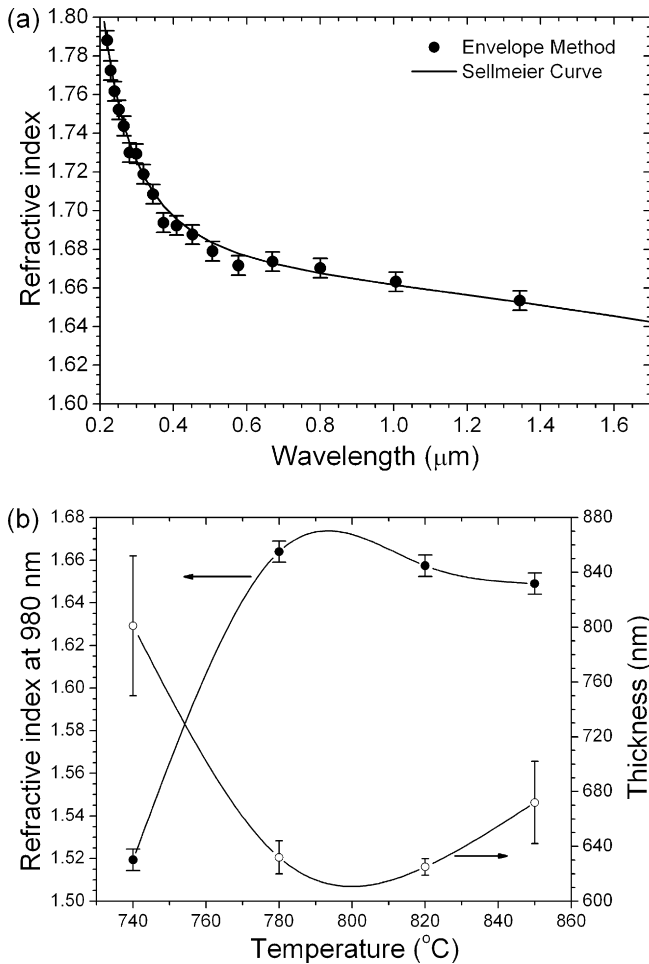


**Fig. 6.** (a) Refractive index dispersion for  $\text{Y}_{0.9}\text{Er}_{0.1}\text{Al}_3(\text{BO}_3)_4$  film on silica substrate and annealed at 780 °C determined by the envelope method in comparison with the Sellmeier curve. (b) Refractive index at  $\lambda = 980$  nm and thickness of  $\text{Y}_{0.9}\text{Er}_{0.1}\text{Al}_3(\text{BO}_3)_4$  thin films on silica substrate, annealed at different temperatures with a heating rate of 2 °C/min. The lines in (b) are used to guide the eyes.

**Table 2**  
Packing densities for the films annealed at different temperatures, calculated from the extraordinary index of Er:YAB crystals.

	Annealing temperature (°C)			
	740	780	820	850
Packing density	0.76	0.96	0.95	0.94

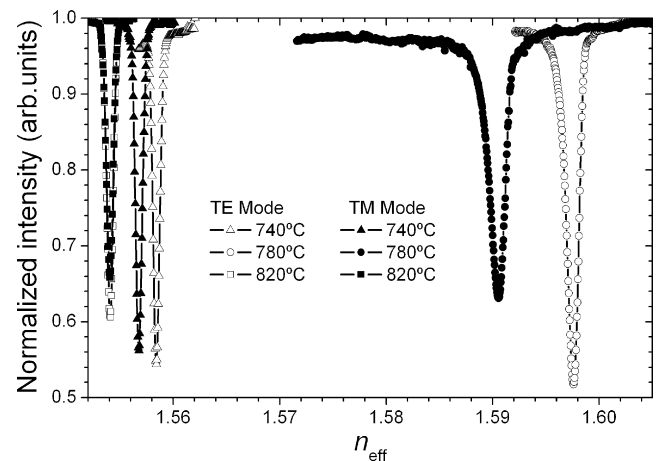


**Fig. 7.** Normalized spectra of TE and TM guided modes for  $\text{Y}_{0.9}\text{Er}_{0.1}\text{Al}_3(\text{BO}_3)_4$  thin films coated on silica substrate. Spectra were obtained by measuring the reflected intensity versus the incidence angle.

**Table 3**

Values of effective indexes, coupling intensity, FWHM, and refractive indexes computed for TE<sub>0</sub> and TM<sub>0</sub> guided modes.

	Mode	Annealing temperature (°C)		
		740	780	820
Effective index ( $n_{\text{eff}}$ ) ( $\pm 0.0005$ )	TE <sub>0</sub>	1.5584	1.5976	1.5541
	TM <sub>0</sub>	1.5568	1.5906	1.5541
Coupling intensity (%)	TE <sub>0</sub>	46	48	39
	TM <sub>0</sub>	44	37	34
$m$ -Line FWHM ( $\pm 0.0005$ )	TE <sub>0</sub>	0.0007	0.0013	0.0007
	TM <sub>0</sub>	0.0007	0.0017	0.0007
Computed refractive index ( $\pm 0.0005$ )		1.5736	1.6354	1.5552

thin film quality. The film refractive indexes, calculated from the effective ones, are 1.5736 at 740 °C, 1.6354 at 780 °C and 1.5552 at 820 °C. These refractive index values are similar to those previously calculated by the envelope method.

The propagation losses of 15 mm long Y<sub>0.9</sub>Er<sub>0.1</sub>Al<sub>3</sub>(BO<sub>3</sub>)<sub>4</sub> glassy waveguides for the TE<sub>0</sub> mode excited at 632.8 nm are around 0.86 ± 0.11 dB/cm. The Y<sub>0.9</sub>Er<sub>0.1</sub>Al<sub>3</sub>(BO<sub>3</sub>)<sub>4</sub> waveguides exhibit a single propagation mode in the third telecommunication window (1550 nm) with an attenuation coefficient of about 0.88 ± 0.21 dB/cm. Similar results are found for other systems (0.8 dB/cm) [27,28]. As the propagation losses of the glassy planar waveguides are relatively low, it is reasonable to consider them for integrated optical devices. Moreover, the spectroscopic properties of the erbium-doped waveguides, which were presented in previous work [29], suggest their possible use in optical amplification. Further work will, however, be necessary because of the high boron content which affects the emission efficiency due to multi-phonon non-radiative relaxation.

Comparing the results reported in this work with those ones mentioned in another work developed by our group [24], we note that the films from the sol-gel process possess superior quality to those prepared from the polymeric precursor (PP) method. The refractive index of the films obtained from sol-gel (SG) process is higher than those from PP method. Thus, the SG method leads the formation of a more cross-linked glass structure with a higher density than that resulting from the PP syntheses. These main differences between the refractive index of the thin films from the SG and PP methods can be explained in terms of the structural arrangements and relative quantities of BO<sub>3</sub> and BO<sub>4</sub> units. It is known that higher BO<sub>4</sub> unit quantities leads to a more connected glassy network and dense structure in agreement with a higher refractive index for the Er:YAB thin films from sol-gel process than that ones from the polymeric precursor method [13,24,30].

#### 4. Conclusions

Y<sub>0.9</sub>Er<sub>0.1</sub>Al<sub>3</sub>(BO<sub>3</sub>)<sub>4</sub> glassy thin films were synthesized by the sol-gel process. The structural, microstructural, and optical properties of the films were optimized for best waveguiding properties. Through a seven multi-layer process we obtained dense thin films, around 620 nm thick, without cracks, voids, grains or porosities for an annealing at 780 °C. The Y<sub>0.9</sub>Er<sub>0.1</sub>Al<sub>3</sub>(BO<sub>3</sub>)<sub>4</sub> thin films are amorphous until 780 °C, while their crystallization starts at 820 °C with the formation of the Al<sub>4</sub>B<sub>2</sub>O<sub>9</sub> phase followed by that of YBO<sub>3</sub> at higher temperature (850 °C). The film roughness measured for these optimized thin films is 0.1 nm RMS, which is very promising for the preparation of low optical loss devices. The films exhibited a

good transparency (higher than 85%) in the near UV-Vis-near IR regions with good interference spectra for those annealed at 780 and 820 °C. The Sellmeier curve could thus be determined. Finally, best films, annealed at 780 °C, showed good waveguiding properties with high light-coupling efficiency (~48%) and higher refractive index ~1.664 at 980 nm. Direct measurement of the waveguide losses showed values of 0.86 dB/cm for 632.8 nm and 0.88 dB/cm for 1550 nm. These values are close to published values for other systems such as SiO<sub>2</sub>-HfO<sub>2</sub>-Er<sub>2</sub>O<sub>3</sub> and SiO<sub>2</sub>-ZrO<sub>2</sub>-Er<sub>2</sub>O<sub>3</sub> [28,31]. These results revealed that our rare earth aluminoborate (Y<sub>0.9</sub>Er<sub>0.1</sub>Al<sub>3</sub>(BO<sub>3</sub>)<sub>4</sub>) host exhibit potential waveguide developments.

#### Acknowledgements

The authors thank the financial support from FAPESP (No. 02/13748-9) and CAPES (No. 455/04-1) Brazilian agencies and CAPES-COFECUB French-Brazilian agreement (No. 455/04).

#### References

- [1] P.G. Kik, A. Polman, MRS Bull. 23 (1998) 48.
- [2] O.H. Park, S.J. Kim, B.S. Bae, J. Mater. Chem. 14 (2004) 1749.
- [3] D.J. Kang, W.S. Kim, B.S. Bae, H.K. Park, B.H. Jung, Appl. Phys. Lett. 87 (2005) 221106.
- [4] J. Qiu, A. Makishima, J. Nanosci. Nanotechnol. 5 (2005) 1541.
- [5] L. Lou, D. Boyer, G. Bertrand-Chadeyron, E. Bernstein, R. Mahiou, J. Mugnier, Opt. Mater. 15 (2000) 1.
- [6] L.J.Q. Maia, C.A.C. Feitosa, F.S. de Vicente, V.R. Mastelaro, M. Siu Li, A.C. Hernandez, J. Vac. Sci. Technol. A 22 (2004) 2163.
- [7] D. Boyer, G. Bertrand-Chadeyron, R. Mahiou, A. Brioude, J. Mugnier, Opt. Mater. 24 (2003) 35.
- [8] M. Tukia, J. Holsa, M. Lastusaari, J. Niittykoski, Opt. Mater. 27 (2005) 1516.
- [9] J. Liao, Y. Lin, Y. Chen, Z. Luo, Y. Huang, J. Cryst. Growth. 267 (2004) 134.
- [10] T.H. Hoekstra, P.V. Lambeck, H. Albers, Th.J.A. Popma, Electron. Lett. 29 (1993) 581.
- [11] L.J.Q. Maia, V.R. Mastelaro, S. Pairis, A.C. Hernandez, A. Ibanez, J. Solid State Chem. 180 (2007) 611.
- [12] T.R. Giraldo, C. Ribeiro, M.T. Escote, T.G. Conti, A.J. Chiquito, E.R. Leite, E. Longo, J.A. Varela, J. Nanosci. Nanotechnol. 6 (2006) 3849.
- [13] L.J.Q. Maia, C.R. Ferrari, V.R. Mastelaro, A.C. Hernandez, A. Ibanez, Solid State Sci. 10 (2008) 1835.
- [14] P.K. Tien, R. Ulrich, J. Opt. Soc. Am. 60 (1970) 1325.
- [15] J. Madarasz, E. Beregi, J. Sztatisz, I. Foldvari, G. Pokol, J. Therm. Anal. Calorim. 64 (2001) 1059.
- [16] L.J.Q. Maia, A. Ibanez, L. Ortega, V.R. Mastelaro, A.C. Hernandez, J. Nanopart. Res. 10 (2008) 1251.
- [17] C.E. Weir, R.A. Schroeder, J. Res. Natn. Bur. Stand. A 68 (1964) 465.
- [18] K. El-Egili, Physica B 325 (2003) 340.
- [19] D. Mazza, M. Vallino, G. Busca, J. Am. Ceram. Soc. 75 (1992) 1929.
- [20] J.C. Manificier, J. Gasiot, J.P. Fillard, J. Phys. E 9 (1976) 1002.
- [21] C.H. Peng, S.B. Desu, J. Am. Ceram. Soc. 77 (1994) 929.
- [22] O.V. Mazurin, M.V. Streltsina, T.P. Shvaiko-Shvaikovskaya, Handbook of Glass Data: Part A – Silica Glass and Binary Silicate Glasses, Elsevier, New York, 1983.
- [23] R. Martínez Vázquez, R. Osellame, M. Marangoni, R. Ramponi, E. Diéguez, Opt. Mater. 26 (2004) 231.
- [24] L.J.Q. Maia, A. Ibanez, J. Fick, N. Sanz, A.C. Hernandez, V.R. Mastelaro, J. Nanosci. Nanotechnol. 7 (2007) 3629.
- [25] D.A.G. Bruggeman, The calculation of various physical constants of heterogeneous substances. I. The dielectric constants and conductivities of mixtures composed of isotropic substances, Ann. Phys. (Leipzig) 24 (1935) 636.
- [26] R. Ulrich, R. Torge, Appl. Opt. 12 (1973) 2901.
- [27] S. Taccheo, G. Della Valle, R. Osellame, G. Cerullo, N. Chiodo, P. Laporta, O. Svelto, A. Killi, U. Morgner, M. Lederer, D. Kopf, Opt. Lett. 29 (2004) 2626.
- [28] R.R. Gonçalves, G. Carturan, M. Montagna, M. Ferrari, L. Zampedri, S. Pelli, G.C. Righini, S.J.L. Ribeiro, Y. Messaddeq, Opt. Mater. 25 (2004) 131.
- [29] L.J.Q. Maia, V.R. Mastelaro, A.C. Hernandez, J. Fick, A. Ibanez, Thin Solid Films, 2009, doi:10.1016/j.tsf.2009.04.040.
- [30] L.J.Q. Maia, Síntese e Caracterização de Filmes Finos do Sistema Y<sub>2</sub>O<sub>3</sub>-Er<sub>2</sub>O<sub>3</sub>-Al<sub>2</sub>O<sub>3</sub>-B<sub>2</sub>O<sub>3</sub> para Aplicação como Amplificadores ópticos Planares, Ph.D. Thesis (co-tutelage) – IFSC/USP (Brazil) and CNRS/UJF (France), 2006.
- [31] R.R. Gonçalves, J.J. Guimarães, J.L. Ferrari, L.J.Q. Maia, S.J.L. Ribeiro, J. Non-Cryst. Solids 354 (2008) 4846.